

Hierarchical Lorentz Mirror Model: Normal Transport and a Universal 2/3 Mean–Variance Law

Raphaël Lefevere^{1,*} and Hal Tasaki^{2,†}

¹*Laboratoire de Probabilités, Statistiques et Modélisation, Université Paris Cité*

²*Department of Physics, Gakushuin University, Mejiro, Toshima-ku, Tokyo 171-8588, Japan*

(Dated: February 10, 2026)

The Lorentz mirror model provides a clean setting to study macroscopic transport generated solely by quenched environmental randomness. We introduce a hierarchical version that admits an exact recursion for the distribution of left–right crossings, and prove normal transport: the mean conductance scales as (cross-section)/(length) for all length scales if $d \geq 3$. A Gaussian approximation, supported by numerics, predicts that, in the marginal case $d = 2$, this scaling acquires a logarithmic correction and that the variance-to-mean ratio of conductance converges to the universal value 2/3 (the “2/3 law”) for all $d \geq 2$. We conjecture that both effects persist beyond the hierarchical setting. We finally provide numerical evidence for the 2/3 law in the original Lorentz mirror model in $d = 3$, and interpret it as a universal signature of normal transport induced by random current matching.

A YouTube video discussing the background and the main results of the paper is available:
<https://youtu.be/G1nqKd6MiXo>

Deriving macroscopic normal transport—as described by diffusive laws such as Fick’s, Ohm’s, and Fourier’s laws—from microscopic deterministic dynamics remains a central challenge in nonequilibrium statistical mechanics [1–4]. Lorentz-type models, in which particles move deterministically through an externally imposed (often disordered) environment, provide a natural testing ground for this program [5–7]. The Lorentz mirror model introduced by Ruijgrok and Cohen [9] is a particularly clean lattice realization: local scattering is deterministic, so any normal transport must be generated by quenched environmental randomness rather than by stochastic forcing or chaotic microscopic dynamics [8–21].

In the present Letter, we propose and study a hierarchical version of the Lorentz mirror model. We rigorously establish normal transport in dimensions $d \geq 3$, and conjecture weakly anomalous transport with a logarithmic correction in the marginal case $d = 2$. Most strikingly, we conjecture that the ratio of the sample-to-sample variance of the conductance to its mean approaches the universal value 2/3 not only in the hierarchical model but also in the original mirror model, suggesting a novel universal signature of normal transport induced by random current matching. A video discussing the background and the main results of the paper is available [22].

Original Lorentz mirror model.— Let us describe the Lorentz mirror model, starting with $d = 2$. Consider the $L \times L$ square lattice with periodic boundary conditions in the vertical direction and open boundary conditions in the horizontal direction. We attach one external edge to each boundary vertex on the left and on the right (thick lines in Fig. 1), so that every vertex has four incident edges. (This particular geometry, suited to the study of transport properties, was first introduced in [16].) At each vertex, we independently choose one of the three pairings of the four incident edges, each with probability

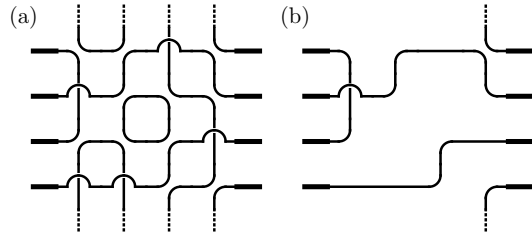


FIG. 1. Original Lorentz mirror model in $d = 2$ (periodic boundary conditions in the vertical direction). (a) A random choice of local pairings yields a collection of disjoint trajectories. (b) The induced perfect matching of the external edges (thick lines). There are two crossings.

1/3. These local pairings decompose the edges into a collection of disjoint trajectories and induce a global perfect matching of the external edges; see Fig. 1. As the name suggests, in $d = 2$ the local pairing may be viewed as arising from reflections by randomly placed mirrors [23].

Similarly, for $d \geq 3$, we consider the d -dimensional $L \times \dots \times L$ hypercubic lattice with open boundary conditions in one (horizontal) direction and periodic boundary conditions in the remaining $d - 1$ directions. We attach L^{d-1} external edges to each of the two open boundaries, and at each vertex independently choose one of the $(2d - 1)!!$ pairings of the $2d$ incident edges with equal probability. (Note that this does not literally correspond to mirror configurations.) Again, the local wiring induces a global perfect matching of the external edges.

Given such a matching of the external edges, a matched pair is said to be a crossing if it connects the left boundary to the right boundary. We denote by \mathcal{C} the number of crossings in a given random environment and call \mathcal{C} the conductance. Its expectation $\bar{\mu}(L) = \langle \mathcal{C} \rangle$ is called the mean conductance (or simply the conductance). This terminology is motivated by the dynamical interpreta-

tion: a particle (or light ray) arriving at a vertex along an incident edge leaves along its paired edge, so trajectories are uniquely determined by the environment. In a nonequilibrium setting where particle baths maintain different densities at the two open boundaries, the stationary current is proportional to \mathcal{C} [16, 17].

Normal transport implies that the mean conductance is proportional to the cross-section $A = L^{d-1}$ of the system divided by its horizontal length L , i.e.,

$$\bar{\mu}(L) \propto A/L = L^{d-2}. \quad (1)$$

For $d = 3$, the scaling (1) is supported by numerical results in [17] and is consistent with the multiscale analysis of [21] based on a closure assumption on trajectory correlations.

Note that (1) would follow readily if the particle motion were diffusive in the usual sense (e.g., well approximated by a random walk). However, the microscopic motion in the Lorentz mirror model is far from diffusive: for large L a substantial fraction of vertices lie on closed orbits [10, 20]; see also Fig. 1 (a). Nevertheless, any particle injected through an external edge necessarily exits through an external edge by construction. A full probabilistic understanding of the model—and a rigorous derivation of (1)—appears to be a formidable task. We nonetheless expect that, on large scales, the model exhibits universal features that are captured by the idealized coarse-grained model introduced in this Letter.

The hierarchical model.— We follow the tradition of hierarchical models in statistical mechanics [24–32] and introduce a hierarchical version of the Lorentz mirror model, in which coarse-graining is implemented explicitly and is amenable to analysis. Our construction is inspired by the multiscale “slab concatenation” viewpoint developed for the original Lorentz mirror model in [21].

We define the model in dimensions $d = 1, 2, \dots$. Fix a positive even integer A_0 . A generation- n block ($n = 0, 1, 2, \dots$) has $A_n := A_0 2^{(d-1)n}$ external edges on each of its left and right sides, and horizontal length $L_n := 2^n$.

The generation-0 block is defined by matching each left external edge with a right external edge, so that it has exactly A_0 crossings; see Fig. 2 (a). For $n \geq 1$, the generation- n block is constructed from 2^d independent copies of the generation- $(n-1)$ block, arranged as a $2 \times \dots \times 2$ array in d dimensions, as illustrated in Fig. 2 (b). We group 2^{d-1} copies in parallel to form the left half and 2^{d-1} copies in parallel to form the right half. The $A_n = 2^{d-1}A_{n-1}$ external edges on the far left (respectively, far right) become the left (respectively, right) external edges of the generation- n block. The remaining $2A_n = 2^dA_{n-1}$ external edges at the interface between the two halves are then paired uniformly at random, i.e., we choose one of the $(2A_n - 1)!!$ perfect matchings with equal probability. This completes the generation- n block; see Fig. 2 (b).

The internal random wiring induces a perfect matching of the $2A_n$ external edges of the generation- n block.

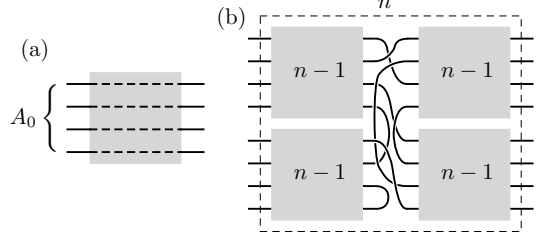


FIG. 2. (a) The generation-0 block. (b) The construction of the generation- n block from 2^d independent copies of the generation- $(n-1)$ block.

Again, a crossing is a matched pair connecting opposite sides. Note that the number of crossings is always even, since the matching at the interface preserves the parity.

Let $P_n(\ell)$, where $\ell \in 2\mathbb{Z}_{\geq 0}$, denote the probability that the generation- n block has exactly ℓ crossings. For any $f(\ell)$, we write $\langle f(\hat{\ell}) \rangle_n := \sum_{\ell} f(\ell) P_n(\ell)$, where $\hat{\ell}$ denotes the (random) number of crossings in the generation- n block. In particular, we set $\mu_n := \langle \hat{\ell} \rangle_n$ and call it the mean conductance (or simply the conductance).

The distribution P_n is determined by the initial condition $P_0(\ell) = \delta_{\ell, A_0}$ and, for $n \geq 1$, the recursion

$$P_n(\ell) = \sum_{\ell_1, \dots, \ell_{2^d}} K(\ell | \ell_L, \ell_R) \prod_{j=1}^{2^d} P_{n-1}(\ell_j), \quad (2)$$

where the sum is over nonnegative even $\ell_1, \dots, \ell_{2^d}$, and $\ell_L = \sum_{j=1}^{2^{d-1}} \ell_j$ and $\ell_R = \sum_{j=2^{d-1}+1}^{2^d} \ell_j$ are the numbers of crossings in the left and right halves, respectively. The kernel $K(\ell | \ell_L, \ell_R)$ is the conditional probability that the random matching at the interface produces exactly ℓ left-right pairs among the $\ell_L + \ell_R$ interface edges that are endpoints of crossings in the generation- $(n-1)$ subblocks, and is given by

$$K(\ell | \ell_L, \ell_R) = \frac{(\ell_L - \ell - 1)!! (\ell_R - \ell - 1)!!}{(\ell_L + \ell_R - 1)!!} \binom{\ell_L}{\ell} \binom{\ell_R}{\ell} \ell!, \quad (3)$$

if $\ell \in S(\ell_L, \ell_R)$, and $K(\ell | \ell_L, \ell_R) = 0$ otherwise, where $S(a, b) := 2\mathbb{Z} \cap [0, \min\{a, b\}]$. It is normalized as $\sum_{\ell \in S(\ell_L, \ell_R)} K(\ell | \ell_L, \ell_R) = 1$. This follows by observing that the uniform random matching of all $2A_n$ interface edges induces, by permutation symmetry, a uniform random matching of the $\ell_L + \ell_R$ distinguished endpoints, and then counting the matchings with exactly ℓ left-right pairs. See below for details.

For fixed ℓ_L and ℓ_R , the conditional mean and variance of $\hat{\ell}$ are

$$\tilde{\mu}(\ell_L, \ell_R) := \sum_{\ell \in S(\ell_L, \ell_R)} \ell K(\ell | \ell_L, \ell_R) = \frac{\ell_L \ell_R}{\ell_L + \ell_R - 1}, \quad (4)$$

and

$$\tilde{v}(\ell_L, \ell_R) = \frac{2\ell_L \ell_R (\ell_L - 1)(\ell_R - 1)}{(\ell_L + \ell_R - 3)(\ell_L + \ell_R - 1)^2}. \quad (5)$$

See End Matter and [23].

Detailed derivation of (3).— To derive (3), fix wirings inside the generation- $(n-1)$ subblocks that have ℓ_L and ℓ_R crossings in the left and right halves. Among the A_n interface edges adjacent to the left half, exactly ℓ_L are endpoints of crossings in the left half, while the remaining $A_n - \ell_L$ interface edges are paired within the left half (“U-turns”). Similarly, among the A_n interface edges adjacent to the right half, ℓ_R are endpoints of crossings and $A_n - \ell_R$ belong to U-turns. The uniform random perfect matching of the $2A_n$ interface edges, together with these fixed U-turn matchings inside the two halves, induces a matching of the $\ell_L + \ell_R$ distinguished endpoints (those belonging to crossings): starting from such an endpoint, follow the interface matching, then (if necessary) follow the prescribed U-turn in that half, and continue until another distinguished endpoint is reached. By permutation symmetry, the induced matching is uniform among all perfect matchings of the $\ell_L + \ell_R$ distinguished edges.

There are $(\ell_L + \ell_R - 1)!!$ perfect matchings of $\ell_L + \ell_R$ labeled endpoints. To obtain exactly ℓ left-right pairs among them, we choose the ℓ endpoints on each side that participate in left-right pairs $\binom{\ell_L}{\ell} \binom{\ell_R}{\ell}$ choices), pair them across ($\ell!$ choices), and pair the remaining $\ell_L - \ell$ left endpoints and $\ell_R - \ell$ right endpoints among themselves to form U-turns (in $(\ell_L - \ell - 1)!!$ and $(\ell_R - \ell - 1)!!$ ways, respectively, with the convention $(-1)!! = 1$). Dividing by $(\ell_L + \ell_R - 1)!!$ yields (3).

Normal transport.— When $\ell_L, \ell_R \gg 1$, (4) reduces to a simple suggestive form $1/\tilde{\mu}(\ell_L, \ell_R) \simeq (1/\ell_L) + (1/\ell_R)$, which is reminiscent of the series-resistance formula. Since the dominant contribution to the recursion (2) should come from $\ell_L \simeq \ell_R \simeq 2^{d-1}\mu_{n-1}$, this suggests the recursion $\mu_n \simeq 2^{d-2}\mu_{n-1}$ for the mean conductance. Its solution gives $\mu_n \simeq (2^{d-2})^n \mu_0 = A_n/L_n$, which is precisely the normal-transport scaling (1).

Our main mathematical contribution is a rigorous version of this observation in $d \geq 3$.

Theorem.— Let $d \geq 3$. For sufficiently large A_0 , there are positive constants C_d and C'_d such that

$$C_d \frac{A_n}{L_n} - 1 \leq \mu_n \leq C'_d \frac{A_n}{L_n}, \quad (6)$$

for all n . If $A_0 \gg 1$, one has $C_d \simeq C'_d \simeq 1$, and hence $\mu_n \simeq A_n/L_n$ for all n .

See End Matter for precise constants and the proof. For $d = 3$, any strictly positive even integer A_0 is allowed, and we have $C_3 = 1 - 5/(4A_0)$ and $C'_3 = 1 + 1/(3A_0)$.

As we shall discuss below, we expect logarithmic growth of μ_n in the marginal dimension $d = 2$. We only have an upper bound consistent with the conjecture. See Theorem 1 in End Matter. For $d = 1$, the same A_0/L_n scaling can be proved up to the scale where μ_n becomes $O(1)$; see Proposition 2 in End Matter.

Gaussian heuristic and the 2/3 law.— A useful (and surprisingly accurate) heuristic is obtained by a Gaussian closure: (i) assume that, for sufficiently large n , the probability distribution P_n is well approximated by a Gaussian with mean $\mu_n = \langle \hat{\ell} \rangle_n$ and variance $v_n := \langle (\hat{\ell} - \mu_n)^2 \rangle_n$; (ii) approximate the interface kernel $K(\ell | \ell_L, \ell_R)$ by a Gaussian in ℓ ,

$$K(\ell | \ell_L, \ell_R) \propto \exp\left[-\frac{\{\ell - \tilde{\mu}(\ell_L, \ell_R)\}^2}{2\tilde{v}(\ell_L, \ell_R)}\right], \quad (7)$$

with the conditional mean $\tilde{\mu}(\ell_L, \ell_R)$ and conditional variance $\tilde{v}(\ell_L, \ell_R)$ given above. (In fact, (7) can be proved in an appropriate asymptotic regime.)

Under this closure, the recursion (2) essentially reduces to Gaussian integrals, and for $d \geq 3$ yields the leading recursions

$$\mu_n \simeq 2^{d-2}\mu_{n-1}, \quad v_n \simeq 2^{d-3}\mu_{n-1} + 2^{d-4}v_{n-1}. \quad (8)$$

Here, the two contributions to v_n come from the conditional variance in (7) and from the fluctuations of ℓ_L and ℓ_R , respectively [23].

Remarkably, the ratio v_n/μ_n satisfies the recursion

$$\frac{v_n}{\mu_n} \simeq \frac{1}{2} + \frac{1}{4} \frac{v_{n-1}}{\mu_{n-1}}, \quad (9)$$

which is independent of d . Therefore $v_n/\mu_n \rightarrow 2/3$ as $n \rightarrow \infty$ (the “2/3 law”).

In the marginal case $d = 2$, the leading drift in (8) cancels; retaining the next-order terms predicts a logarithmic growth

$$\mu_n \simeq \frac{n}{12} = \frac{\log L_n}{12 \log 2}, \quad (10)$$

while still $v_n/\mu_n \rightarrow 2/3$; see [23].

Numerical results for the hierarchical model.— We numerically iterated the recursion (2) in $d = 3$ and $d = 2$ to test the Gaussian-closure predictions. The agreement is excellent. In $d = 3$, after only a few iterations, the mean conductance μ_n is essentially proportional to L_n , and the ratio v_n/μ_n becomes numerically indistinguishable from $2/3$. In the marginal case $d = 2$, after reducing discreteness effects by starting from a moderately large initial crossing number A_0 , we find that μ_n grows linearly in $n = \log_2 L_n$ with slope consistent with $1/12$, and again v_n/μ_n rapidly locks onto $2/3$. We also observe that the standardized law approaches a Gaussian (in Kolmogorov distance) rapidly in $d = 3$, apparently exponentially in n , whereas in $d = 2$ the convergence is much slower and compatible with a n^{-1} decay. See [23] for details.

The remarkably fast stabilization of v_n/μ_n to $2/3$ suggests viewing this ratio as a universal amplitude ratio, characterizing a universality class that contains the present hierarchical Lorentz mirror model. As we shall

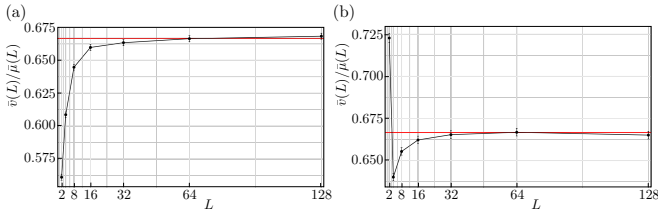


FIG. 3. Ratio $\bar{v}(L)/\bar{\mu}(L)$ of the sample-to-sample variance $\bar{v}(L)$ to the mean $\bar{\mu}(L)$ of the number of crossings, as a function of $L = 2^n$ with $n = 1, \dots, 7$. Error bars indicate 95% confidence intervals. (a) Standard rule (all local pairings allowed). (b) Orthogonal rule (restricted local pairings; no edge is paired with its opposite). The horizontal line marks 2/3.

see below, this expectation is justified, in a stronger sense than we initially anticipated.

Numerical results for the original Lorentz mirror model in $d = 3$.— Normal-transport scaling (1) in the original Lorentz mirror model for $d = 3$ was first supported numerically in [17]. The proportionality constant (conductivity) $\kappa := \lim_{L \uparrow \infty} \bar{\mu}(L)/L$ was derived in [21] from a multiscale analysis under a closure hypothesis on trajectory correlations. This constant is nonuniversal and depends on the microscopic pairing rule.

Here, we report preliminary simulations of the original (non-hierarchical) model aimed at testing the variance-to-mean ratio of the conductance. The results are already strongly suggestive: the ratio $\bar{v}(L)/\bar{\mu}(L)$ rapidly approaches the value 2/3 as L increases, and appears insensitive to microscopic details of the local pairing rule; see Fig. 3. This unexpected robustness leads us to conjecture that the “2/3 law” persists well beyond the hierarchical setting. It is natural to interpret $\bar{v}(L)/\bar{\mu}(L)$ as a universal amplitude ratio for transport problems in which coarse-graining effectively randomizes the matching of conserved currents.

In our simulations, we considered the Lorentz mirror model on the $L \times L \times L$ cubic lattice with two different local pairing rules. The first is the standard rule discussed at the beginning of the Letter. The second is an “orthogonal” rule, in which at each vertex we choose uniformly among the eight local pairings such that no edge is paired with its opposite (equivalently, the velocity of a particle always turns by 90° at each visited vertex).

For each $L = 2^n$ with $n = 1, \dots, 7$ and for each rule, we generated 6.4×10^5 independent quenched random environments (configurations of local pairings). For a given environment, we faithfully evaluated the conductance \mathcal{C} , i.e., the number of left-right crossings, by tracing the deterministic trajectories of particles injected from all L^2 external edges on the left boundary and recording their exit edges. Repeating this procedure over all the environments yields estimates of the mean $\bar{\mu}(L) = \langle \mathcal{C} \rangle$, the variance $\bar{v}(L) := \langle (\mathcal{C} - \bar{\mu}(L))^2 \rangle$, and the ratio $\bar{v}(L)/\bar{\mu}(L)$ with 95% confidence intervals. See [23].

Discussion.— We introduced a hierarchical Lorentz mirror model that captures deterministic transport generated solely by quenched environmental randomness through random matching. For this model, we proved that the conductance exhibits normal-transport scaling, even though the microscopic dynamics is far from diffusive and many trajectories are closed, as in the original mirror model. More precisely, we established that $\mu_n \propto A_n/L_n$ in all dimensions $d \geq 3$. The marginal case $d = 2$ remains open: the Gaussian approximation and numerics suggest that μ_n grows logarithmically with the system size.

A second outcome is the “2/3 law”: whenever μ_n grows with scale, the variance satisfies $v_n/\mu_n \rightarrow 2/3$. In the hierarchical model, this emerges from the Gaussian closure leading to the recursion (9), and is supported numerically. Moreover, we provide numerical evidence that the same ratio holds for the original Lorentz mirror model in $d = 3$, and appears robust under variations of the local pairing rule. This motivates the conjecture that the “2/3 law” is universal within a broad class of models.

Our results suggest that $d = 2$ is the unique marginal dimension of the hierarchical model, and we conjecture the same for the original model. A single injected trajectory may be viewed as a non-backtracking walk with strong memory (encoding the quenched random environment), suggesting a comparison with “true” (myopic) self-avoiding walks and related self-repelling processes, for which $d = 2$ is also marginal and which become diffusive in $d \geq 3$ [33–36]. At the same time, if crossings were produced by essentially independent diffusive trajectories, one would expect Poisson counting statistics, for which v/μ equals 1 rather than approaching the sub-Poisson value 2/3. This contrast suggests that the global current matching—rather than the scaling of an individual trajectory—is the mechanism behind normal transport and the 2/3 law. A rigorous derivation of the 2/3 law, and control of the marginal case $d = 2$, remain important open problems.

Our hierarchical Lorentz mirror model provides a tractable yet still nontrivial setting in which one can study transport phenomena generated by deterministic dynamics in a quenched random environment. There are still many open issues, including a proof of the 2/3 law, that should be studied numerically, theoretically, and mathematically. Needless to say, studying the original Lorentz mirror model is an important direction. From a physics viewpoint, it is most exciting to view the 2/3 law as a novel indicator of a universality class and to examine what models belong to this class. It is particularly interesting to see whether this class contains continuous-space models, as in the original proposal by Lorentz [5].

R.L. thanks Gakushuin University for its hospitality during his stay in Tokyo, when the main part of this work was carried out. He also acknowledges the financial

support from FJ-LMI IRL 2025 CNRS-The University of Tokyo, which made the visit possible. The present research is supported by JSPS Grants-in-Aid for Scientific Research Nos. 22K03474 (R.L. and H.T.) and 25K07171 (H.T.).

We made extensive use of ChatGPT (versions 5.1 and 5.2, Plus/Pro) throughout this project for code development, assistance with proofs and calculations, reference searches, and drafting of the manuscript. In particular, the role of the identity (16) in the proof of Theorem 3 was identified with the assistance of ChatGPT 5.2 Pro (although, interestingly, it never realized (16) until we pointed out that the quantity could be evaluated).

* lefevere@lpsm.paris

† hal.tasaki@gakushuin.ac.jp

- [1] F. Bonetto, J. L. Lebowitz, L. Rey-Bellet, *Fourier's Law: a Challenge for Theorists*, (preprint, 2000).
<https://arxiv.org/abs/math-ph/0002052>
- [2] S. Lepri, R. Livi, A. Politi, *Thermal conduction in classical low-dimensional lattices*, Phys. Rep. **377**, 1–80 (2003).
- [3] A. Dhar, *Heat transport in low-dimensional systems*, Adv. Phys. **57**, 457–537 (2008).
<https://arxiv.org/abs/0808.3256>
- [4] J. L. Lebowitz, H. Spohn, *Microscopic basis for Fick's law for self-diffusion*, J. Stat. Phys. **28**, 539–556 (1982).
- [5] H. A. Lorentz, *The motion of electrons in metallic bodies*, Proc. K. Ned. Akad. Wet. **7**, 438–453 (1905).
- [6] H. van Beijeren, *Transport properties of stochastic Lorentz models*, Rev. Mod. Phys. **54**, 195–234 (1982).
- [7] C. P. Dettmann, *Diffusion in the Lorentz gas*, Commun. Theor. Phys. **62**, 521–540 (2014).
<https://arxiv.org/abs/1402.7010>
- [8] G. Basile, A. Nota, F. Pezzotti, M. Pulvirenti, *Derivation of the Fick's Law for the Lorentz Model in a Low Density Regime*, Commun. Math. Phys. **336**, 1607–1636 (2015).
<https://arxiv.org/abs/1404.4186>
- [9] T. W. Ruijgrok, E. G. D. Cohen, *Deterministic lattice gas models*, Phys. Lett. A **133**, 415–418 (1988).
- [10] L. A. Bunimovich, S. E. Troubetzkoy, *Recurrence properties of Lorentz lattice gas cellular automata*, J. Stat. Phys. **67**, 289–302 (1992).
- [11] L. A. Bunimovich, H. O. Y. Tumarkin, *Topological dynamics of flipping Lorentz lattice gas models*, J. Stat. Phys. **72**, 297–307 (1993).
- [12] E. G. D. Cohen, F. Wang, *New results for diffusion in Lorentz lattice gas cellular automata*, J. Stat. Phys. **81**, 445–466 (1995).
<https://arxiv.org/abs/comp-gas/9501003>
- [13] G. Grimmett, *Percolation*, 2nd ed., Springer, Berlin (1999).
- [14] G. Grimmett and H. Kesten, *Percolation Theory at Saint-Flour*, Springer, Berlin (2012).
- [15] A. S. Kraemer, D. Sanders, *Zero Density of Open Paths in the Lorentz Mirror Model for Arbitrary Mirror Probability*, J. Stat. Phys. **156**, 908–916 (2014).
<https://arxiv.org/abs/1406.4796>
- [16] R. Lefevere, *Fick's law in a random lattice Lorentz gas*, Arch. Ration. Mech. Anal. **216**, 983–1008 (2015).
- [17] Y. Chiffaudel, R. Lefevere, *The Mirrors Model: Macroscopic Diffusion Without Noise or Chaos*, J. Phys. A **49**, 10LT02 (2016).
<https://arxiv.org/abs/1506.04727>
- [18] G. Kozma, V. Sidoravicius, *Lower bound for the escape probability in the Lorentz mirror model on the lattice*, Isr. J. Math. **209**, 683–685 (2015).
<https://arxiv.org/abs/1311.7437>
- [19] K. Ryan, *The Manhattan and Lorentz Mirror Models: A Result on the Cylinder with Low Density of Mirrors*, J. Stat. Phys. **185**, 7 (2021).
<https://link.springer.com/article/10.1007/s10955-021-02837-8>
- [20] D. Elboim, A. Gloria, F. Hernández, *Diffusivity of the Lorentz mirror walk in high dimensions*, preprint (2025).
<https://arxiv.org/abs/2505.01341>
- [21] R. Lefevere, *Multiscale analysis of the conductivity in the Lorentz mirrors model*, preprint (2025).
<https://arxiv.org/abs/2510.24091>
- [22] <https://youtu.be/G1nqKd6MiXo>
- [23] Supplemental Material
- [24] F. J. Dyson, *Existence of a phase-transition in a one-dimensional Ising ferromagnet*, Commun. Math. Phys. **12**, 91–107 (1969).
- [25] P. M. Bleher, Ya. G. Sinai, *Investigation of the critical point in models of the type of Dyson's hierarchical models*, Commun. Math. Phys. **33**, 23–42 (1973).
- [26] G. Gallavotti, H. J. F. Knops, *The hierarchical model and the renormalization group*, Riv. Nuovo Cim. **5**, 341–368 (1975).
- [27] P. Collet, J.-P. Eckmann, *The ϵ -expansion for the hierarchical model*, Commun. Math. Phys. **55**, 67–96 (1977).
- [28] A. N. Berker, S. Ostlund, *Renormalisation-group calculations of finite systems: Order parameter and specific heat for epitaxial ordering*, J. Phys. C: Solid State Phys. **12**, 4961–4975 (1979).
- [29] K. Gawędzki, A. Kupiainen, *A rigorous block spin approach to massless lattice theories*, Commun. Math. Phys. **77**, 31–64 (1980).
- [30] M. Kaufman, R. B. Griffiths, *Exactly soluble Ising models on hierarchical lattices*, Phys. Rev. B **24**, 496–498 (1981).
- [31] K. Gawędzki, A. Kupiainen, *Renormalization group study of a critical lattice model. I. Convergence to the line of fixed points*, Commun. Math. Phys. **82**, 407–433 (1981).
- [32] K. Gawędzki, A. Kupiainen, *Renormalization group study of a critical lattice model. II. The correlation functions*, Commun. Math. Phys. **83**, 469–492 (1982).
- [33] D. J. Amit, G. Parisi, L. Peliti, *Asymptotic behavior of the “true” self-avoiding walk*, Phys. Rev. B **27**, 1635–1645 (1983).
- [34] B. Tóth, *The “true” self-avoiding walk with bond repulsion on \mathbb{Z} : Limit theorems*, Ann. Probab. **23**, 1523–1556 (1995).
- [35] B. Tóth, W. Werner, *The true self-repelling motion*, Probab. Theory Relat. Fields **111**, 375–452 (1998).
https://math.bme.hu/~balint/cikkek/tsrm_ptrf.pdf
- [36] I. Horváth, B. Tóth, B. Vető, *Diffusive limits for “true” (or myopic) self-avoiding random walks and self-repellent Brownian polymers in $d \geq 3$* , Probab. Theory Relat. Fields **153**, 691–726 (2012).
<https://arxiv.org/abs/1009.0401>

END MATTER

We give a complete proof of our main theorem on normal transport, splitting it into Theorems 1 and 3.

Conditional expectation values.— We begin by proving two exact identities, (13) and (16), for conditional expectations. Recall that the kernel is normalized as $\sum_{\ell \in S(a,b)} K(\ell | a, b) = 1$ for any nonnegative even a and b . The combinatorial interpretation of (3) also shows that $\sum_{\ell} K(\ell | a, b) = 1$ when both a and b are odd and positive, where the sum is over odd $\ell \in [1, \min\{a, b\}]$. It is also useful to rewrite (3) as

$$K(\ell | a, b) = \frac{a! b!}{(a+b-1)!! (a-\ell)!! (b-\ell)!! \ell!}. \quad (11)$$

Let a and b be even and positive. Using the above normalization in the odd case (applied to $a-1$ and $b-1$), we have

$$\begin{aligned} 1 &= \sum_{\ell \in S(a,b) \setminus \{0\}} K(\ell-1 | a-1, b-1) \\ &= \sum_{\ell \in S(a,b) \setminus \{0\}} \frac{(a-1)! (b-1)!}{(a+b-3)!! (a-\ell)!! (b-\ell)!! (\ell-1)!} \\ &= \frac{a+b-1}{ab} \sum_{\ell \in S(a,b)} \ell K(\ell | a, b). \end{aligned} \quad (12)$$

This yields the equality in

$$\sum_{\ell \in S(a,b)} \ell K(\ell | a, b) = \frac{ab}{a+b-1} \leq \frac{a+b}{4} + \frac{1}{3}, \quad (13)$$

which proves (4). To prove the upper bound in (13), assume $ab \neq 0$ and set $S := a+b \geq 4$. Then

$$\frac{ab}{a+b-1} - \frac{a+b}{4} = \frac{S - (a-b)^2}{4(S-1)} \leq \frac{S}{4(S-1)} \leq \frac{1}{3}. \quad (14)$$

If $a = 0$ or $b = 0$, the left-hand side of (13) vanishes and the bound is trivial.

Similarly, for even and positive a and b , we find

$$\begin{aligned} 1 &= \sum_{\ell \in S(a,b)} K(\ell+1 | a+1, b+1) \\ &= \sum_{\ell \in S(a,b)} \frac{(a+1)! (b+1)!}{(a+b+1)!! (a-\ell)!! (b-\ell)!! (\ell+1)!} \\ &= \frac{(a+1)(b+1)}{a+b+1} \sum_{\ell \in S(a,b)} \frac{1}{\ell+1} K(\ell | a, b), \end{aligned} \quad (15)$$

which leads to

$$\begin{aligned} \sum_{\ell \in S(a,b)} \frac{1}{\ell+1} K(\ell | a, b) &= \frac{a+b+1}{(a+1)(b+1)} \\ &= (a+1)^{-1} + (b+1)^{-1} - \{(a+1)(b+1)\}^{-1}. \end{aligned} \quad (16)$$

Upper bounds.— For any function $f(a, b)$, define

$$\langle f(\hat{\ell}_L, \hat{\ell}_R) \rangle_n^{\text{LR}} := \sum_{\ell_1, \dots, \ell_{2^d}} f(\ell_L, \ell_R) \prod_{j=1}^{2^d} P_n(\ell_j), \quad (17)$$

where the sum is over nonnegative even $\ell_1, \dots, \ell_{2^d}$, and $\ell_L = \sum_{j=1}^{2^{d-1}} \ell_j$ and $\ell_R = \sum_{j=2^{d-1}+1}^{2^d} \ell_j$. With this notation, the recursion (2) reads $P_n(\ell) = \langle K(\ell | \hat{\ell}_L, \hat{\ell}_R) \rangle_{n-1}^{\text{LR}}$. Recalling $\mu_n = \sum_{\ell} \ell P_n(\ell)$ and using the upper bound in (13), we obtain

$$\mu_n \leq \frac{\langle \hat{\ell}_L + \hat{\ell}_R \rangle_{n-1}^{\text{LR}}}{4} + \frac{1}{3} = 2^{d-2} \mu_{n-1} + \frac{1}{3}, \quad (18)$$

for $n = 1, 2, \dots$, where we used $\langle \hat{\ell}_L \rangle_{n-1}^{\text{LR}} = \langle \hat{\ell}_R \rangle_{n-1}^{\text{LR}} = 2^{d-1} \mu_{n-1}$. For $d \neq 2$, we rewrite this as $(\mu_n + C_d') \leq 2^{d-2} (\mu_{n-1} + C_d'')$ with $C_d'' = \{3(2^{d-2}-1)\}^{-1}$, and obtain the following (remember that $\mu_0 = A_0$).

Theorem 1.— For any $n = 0, 1, \dots$, we have

$$\mu_n \leq \begin{cases} 2^{(d-2)n} (\mu_0 + C_d'') - C_d' = C_d' A_n / L_n - C_d'', & d \neq 2; \\ A_0 + \frac{n}{3} = A_0 + (3 \log 2)^{-1} \log L_n, & d = 2, \end{cases} \quad (19)$$

with constants $C_d' = 1 + C_d''/A_0$.

For $d \geq 3$, where $C_d'' > 0$, this implies the upper bound in (6). Note that the bound for $d = 2$ is consistent with the expected logarithmic growth (10). The bound for $d \neq 2$ is also valid for $d = 1$ with $C_1'' = -2/3$.

Lower bounds.— To prove lower bounds, we introduce

$$\eta_n := \langle (\hat{\ell} + 1)^{-1} \rangle_n = \sum_{\ell} (\ell + 1)^{-1} P_n(\ell). \quad (20)$$

Since $x \mapsto x^{-1}$ is convex, Jensen's inequality yields $\eta_n = \langle (\hat{\ell} + 1)^{-1} \rangle_n \geq 1 / \langle \hat{\ell} + 1 \rangle_n$, and hence $\mu_n \geq \eta_n^{-1} - 1$. Thus an upper bound on η_n implies a lower bound on μ_n .

Moreover, (16) implies the exact identity

$$\begin{aligned} \eta_n &= \langle (\hat{\ell}_L + 1)^{-1} \rangle_{n-1}^{\text{LR}} + \langle (\hat{\ell}_R + 1)^{-1} \rangle_{n-1}^{\text{LR}} \\ &\quad - \langle (\hat{\ell}_L + 1)^{-1} \rangle_{n-1}^{\text{LR}} \langle (\hat{\ell}_R + 1)^{-1} \rangle_{n-1}^{\text{LR}}, \end{aligned} \quad (21)$$

where we noted that $\hat{\ell}_L$ and $\hat{\ell}_R$ are independent in the expectation (17).

As a warm-up, we start from the less interesting case with $d = 1$. Dropping the last (negative) term in (21) and noting $\langle (\hat{\ell}_L + 1)^{-1} \rangle_{n-1}^{\text{LR}} = \langle (\hat{\ell}_R + 1)^{-1} \rangle_{n-1}^{\text{LR}} = \eta_{n-1}$, we obtain $\eta_n \leq 2\eta_{n-1}$, hence $\eta_n \leq 2^n \eta_0 = 2^n / (A_0 + 1)$. We have thus proved the following.

Proposition 2.— For $d = 1$ and any $n = 0, 1, \dots$,

$$\mu_n \geq (A_0 + 1) / L_n - 1. \quad (22)$$

Combined with the upper bound (19), this shows $\mu_n \simeq A_0 / L_n$ for $d = 1$, as long as $A_0 \gg 1$ and μ_n remains much

larger than unity. This may be regarded as (a weak form of) normal transport in the limited length scale.

For $d \geq 3$, we prove a lower bound with the correct scaling in the same spirit. Let us first discuss a rough argument and state the theorem. Define

$$u_n := \langle (\hat{\ell}_L + 1)^{-1} \rangle_n^{\text{LR}} = \langle (\hat{\ell}_R + 1)^{-1} \rangle_n^{\text{LR}}, \quad (23)$$

where the equality follows from symmetry. (Note that $u_n = \eta_n$ when $d = 1$.) Then (21) implies the identity

$$\eta_n = 2u_{n-1} - (u_{n-1})^2. \quad (24)$$

A further estimate based on concavity (proved below) yields

$$u_n \leq \frac{\eta_n}{2^{d-1} - (2^{d-1} - 1)\eta_n}. \quad (25)$$

Combining this with (24), we arrive at the recursive inequality

$$\eta_n \leq 2^{2-d} \eta_{n-1} + (1 - 2^{1-d})^2 (\eta_{n-1})^2. \quad (26)$$

Iterating this inequality and using $\mu_n \geq \eta_n^{-1} - 1$, we obtain the following.

Theorem 3.— For $d \geq 3$, one has

$$\mu_n \geq C_d A_n / L_n - 1, \quad (27)$$

for any $n = 0, 1, \dots$, with a constant

$$C_d = 1 - \frac{1}{A_0} \left(\frac{(2^{d-1} - 1)^2}{2(2^{d-1} - 2)} - 1 \right), \quad (28)$$

where we take A_0 sufficiently large so that $C_d > 0$.

Proof of Theorem 3.— We discuss the case $d = 3$; the extension to general $d \geq 3$ is straightforward [23]. From (23) and (17), we have

$$u_n = \sum_{\ell_1, \dots, \ell_4} \left(1 + \sum_{j=1}^4 \ell_j \right)^{-1} \prod_{j=1}^4 P_n(\ell_j), \quad (29)$$

where the sum is over nonnegative even ℓ_1, \dots, ℓ_4 (we have summed over ℓ_5, \dots, ℓ_8). Make the change of variables $y = (\ell + 1)^{-1} \in (0, 1]$ and define $Q_n(y) = P_n(y^{-1} - 1)$. Then $\eta_n = \sum_y y Q_n(y)$ and (29) becomes

$$u_n = \sum_{y_1, \dots, y_4} \left(\sum_{j=1}^4 y_j^{-1} - 3 \right)^{-1} \prod_{j=1}^4 Q_n(y_j). \quad (30)$$

Fix $y_2, y_3, y_4 \in (0, 1]$ and set $c := \sum_{j=2}^4 y_j^{-1} - 3 \geq 0$. The function $(y_1^{-1} + c)^{-1} = y_1/(1 + cy_1)$ is concave in $y_1 \in (0, 1]$, since its second derivative equals $-2c(1 + cy_1)^{-3} \leq 0$. By Jensen's inequality,

$$u_n \leq \sum_{y_2, y_3, y_4} \left(\eta_n^{-1} + \sum_{j=2}^4 y_j^{-1} - 3 \right)^{-1} \prod_{j=2}^4 Q_n(y_j), \quad (31)$$

and repeating the same argument for y_2, y_3, y_4 yields $u_n \leq (4\eta_n^{-1} - 3)^{-1} = \eta_n/(4 - 3\eta_n)$. Substituting this (with $n \mapsto n - 1$) into (24), we find

$$\eta_n \leq \frac{8\eta_{n-1} - 7\eta_{n-1}^2}{(4 - 3\eta_{n-1})^2}. \quad (32)$$

Noting that

$$\frac{8\eta - 7\eta^2}{(4 - 3\eta)^2} - \left(\frac{\eta}{2} + \frac{9}{16}\eta^2 \right) = -\frac{\eta^2(9\eta - 8)^2}{16(4 - 3\eta)^2} \leq 0, \quad (33)$$

we obtain the recursive inequality

$$\eta_n \leq \frac{\eta_{n-1}}{2} + \frac{9}{16}\eta_{n-1}^2. \quad (34)$$

It remains to iterate (34). Set $x_n = 2^n \eta_n$. Then (34) implies

$$x_n \leq x_{n-1} + \frac{9}{8} 2^{-(n-1)} x_{n-1}^2, \quad (35)$$

and therefore

$$\frac{1}{x_n} \geq \frac{1}{x_0} - \frac{9}{8} 2^{-(n-1)}, \quad (36)$$

since $(x + ax^2)^{-1} \geq x^{-1} - a$ for $x > 0$ and $a \geq 0$. Summing over n and using $x_0 = \eta_0 = (A_0 + 1)^{-1}$, we obtain

$$\frac{1}{x_n} \geq \frac{1}{x_0} - \frac{9}{8} \sum_{k=0}^{n-1} 2^{-k} \geq (A_0 + 1) - \frac{9}{4} = A_0 - \frac{5}{4}. \quad (37)$$

Thus $\eta_n^{-1} \geq (A_0 - \frac{5}{4})2^n$, and hence $\mu_n \geq \eta_n^{-1} - 1 \geq (A_0 - \frac{5}{4})L_n - 1$, which is the desired bound (27). ■

Supplemental Material for “Hierarchical Lorentz Mirror Model: Normal Transport and a Universal 2/3 Mean–Variance Law”

Raphaël Lefevere and Hal Tasaki

In this Supplemental Material, we collect background information, straightforward but somewhat involved computations and extensions, as well as details of our numerical simulations. These materials are intended for interested readers; the main text of the Letter, together with the End Matter, is self-contained.

Specifically, we discuss the relation between the traditional “mirror” formulation and the local-pairing formulation used in the main text (Sec. SM.1), details of the Gaussian closure (Sec. SM.2), the extension of the proof of Theorem 3 to general dimensions $d \geq 3$ (Sec. SM.3), and additional information on our numerical simulations (Sec. SM.4).

SM.1 From mirrors to local pairings

Here, we explain the precise relation, in $d = 2$, between the traditional “mirror” formulation of the Lorentz mirror model and the “tube” (local-pairing) formulation used in the main text.

Fix $L \in \mathbb{N}$ and let

$$\Lambda := \{1, 2, \dots, L\} \times \{1, 2, \dots, L\}, \quad (\text{SM.1})$$

be the $L \times L$ square lattice. We consider the nearest-neighbor graph on Λ with periodic boundary conditions in the second (vertical) coordinate and open boundary conditions in the first (horizontal) coordinate. More precisely, for $(x, y) \in \Lambda$, we connect (x, y) to $(x, y \pm 1)$ with $y \pm 1$ understood modulo L , and to $(x \pm 1, y)$ provided $x \pm 1 \in \{1, 2, \dots, L\}$. We then attach one external edge to each boundary vertex on the left ($x = 1$) and on the right ($x = L$), so that every vertex has four incident edges. In Fig. SM.1 (a) and (c), periodic boundary conditions are indicated by dotted lines, and the added external edges are depicted in thick lines.

A mirror configuration assigns to each vertex $(x, y) \in \Lambda$ one of three local scatterers: an empty site (no mirror), a “/” mirror, or a “\” mirror. See Fig. SM.1 (a). A particle (or light ray) moves deterministically along edges: when it arrives at a vertex along one incident edge, it leaves along the edge prescribed by the local scatterer.

Since the scattering is time-reversal invariant, each local rule induces a pairing of four incident edges to the vertical. Concretely, if we label the four incident edges by the cardinal directions $\{N, E, S, W\}$, the three local rules are equivalent to the three pairings as follows. See also Fig. SM.1 (b).

$$(\text{empty}) \iff \{\{W, E\}, \{N, S\}\}, \quad (/ \text{ mirror}) \iff \{\{W, N\}, \{E, S\}\}, \quad (\backslash \text{ mirror}) \iff \{\{W, S\}, \{E, N\}\}. \quad (\text{SM.2})$$

Thus, a mirror configuration is exactly the same object as an assignment, to each vertex, of one of the three pairings of its four incident edges. See Fig. SM.1 (c). This is nothing but the definition of the model presented in the main text.

One can attempt to generalize the mirror picture to $d \geq 3$ by placing geometric reflectors (e.g., mirror planes) at each vertex and letting particles undergo specular reflection. However, such geometric reflections realize only a restricted subset of the possible pairings of the $2d$ incident lattice edges. In particular, for $d = 3$ there are $(2d - 1)!! = 15$ pairings of the six incident edges, whereas mirror-plane reflections acting on the coordinate directions generate only a proper subset. For this reason, a literal “mirror” construction in $d \geq 3$ does not coincide with the simple and natural local-pairing model adopted in the main text, where each of the $(2d - 1)!!$ pairings is chosen with equal probability.

SM.2 Gaussian closure: derivation of (8) and the 2/3 law

We record the computations behind the Gaussian heuristic quoted in the main text.

SM.2.1 Conditional mean/variance of the interface matching

Fix nonnegative integers a, b and consider a uniform perfect matching of $a + b$ labeled interface edges, where a edges are marked L and b edges are marked R. Let $\Lambda(a, b)$ be the number of L–R pairs created by this matching. Introduce indicators I_i ($i = 1, \dots, a$) that equal 1 iff the i -th L edge is paired to an R edge. Then $\Lambda(a, b) = \sum_{i=1}^a I_i$ and by symmetry

$$\langle I_i \rangle = \frac{b}{a + b - 1}, \quad (\text{SM.1})$$

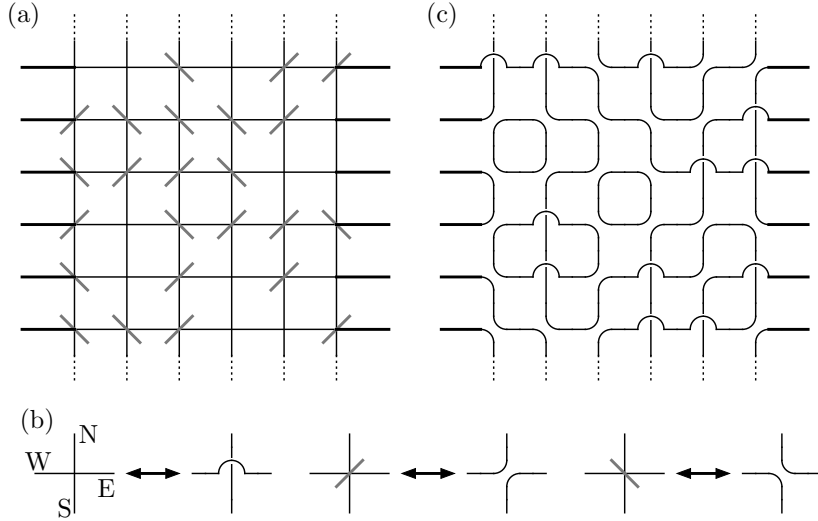


FIG. SM.1. Equivalence between the mirror and tube representations in $d = 2$. (a) A configuration of mirrors (empty sites, “/” mirrors, and “\” mirrors) on the $L \times L$ square lattice with periodic boundary conditions vertically and external edges attached on the left and right. (b) Local correspondence between the three vertex types (empty, “/” mirror, and “\” mirror) and the three pairings of the four incident edges. (c) The corresponding tube/trajectory picture obtained by translating each local mirror choice into a pairing of the four incident edges; the disjoint trajectories induce a perfect matching of the external edges.

so

$$\tilde{\mu}(a, b) := \langle \Lambda(a, b) \rangle = \frac{ab}{a + b - 1}. \quad (\text{SM.2})$$

For $i \neq j$, after fixing one L–R matching there remain $a + b - 3$ possible partners for the other L edge, of which $b - 1$ are R, hence

$$\langle I_i I_j \rangle = \frac{b}{a + b - 1} \frac{b - 1}{a + b - 3}. \quad (\text{SM.3})$$

Therefore $\langle \Lambda(\Lambda - 1) \rangle = a(a - 1)b(b - 1)/\{(a + b - 1)(a + b - 3)\}$ and

$$\tilde{v}(a, b) := \text{Var}(\Lambda(a, b)) = \frac{2ab(a - 1)(b - 1)}{(a + b - 3)(a + b - 1)^2}. \quad (\text{SM.4})$$

For $a \simeq b$ large, $\tilde{v}(a, b) = 2a^2b^2/(a + b)^3\{1 + O(a^{-1} + b^{-1})\}$, so in particular $\tilde{v}(\nu, \nu) = \nu/4 + O(1)$ for $\nu \gg 1$.

SM.2.2 Input statistics at scale $n - 1$

Let $m := 2^{d-1}$. In the recursion (2), $\ell_L = \sum_{j=1}^m \ell_j$ and $\ell_R = \sum_{j=m+1}^{2m} \ell_j$, where ℓ_j are assumed to be i.i.d. with Gaussian law P_{n-1} with parameters (μ_n, v_n) . Thus

$$\langle \ell_L \rangle = \langle \ell_R \rangle = m\mu_{n-1}, \quad \text{Var}(\ell_L) = \text{Var}(\ell_R) = mv_{n-1}, \quad (\text{SM.5})$$

and ℓ_L and ℓ_R are independent.

SM.2.3 Mean recursion for $d \geq 3$

Under the Gaussian closure, we assume that P_{n-1} is a (discrete) Gaussian with mean μ_{n-1} and variance v_{n-1} of the same order of magnitude. We find an approximate recursion relation for $\mu_n = \langle \tilde{\mu}(\ell_L, \ell_R) \rangle$ by expanding $\tilde{\mu}(a, b) = ab/(a + b - 1)$ around the symmetric point $(a, b) = (m\mu_{n-1}, m\mu_{n-1})$. We assume μ_{n-1} large and the leading term gives

$$\begin{aligned} \mu_n &\simeq \tilde{\mu}(m\mu_{n-1}, m\mu_{n-1}) \\ &= \frac{m^2\mu_{n-1}^2}{2m\mu_{n-1} - 1} \simeq \frac{m}{2}\mu_{n-1} = 2^{d-2}\mu_{n-1}. \end{aligned} \quad (\text{SM.6})$$

SM.2.4 Variance recursion for $d \geq 3$

By the law of total variance,

$$v_n = \langle \tilde{v}(\ell_L, \ell_R) \rangle + \text{Var}(\tilde{\mu}(\ell_L, \ell_R)). \quad (\text{SM.7})$$

For the intrinsic term, evaluating (SM.4) at $(m\mu_{n-1}, m\mu_{n-1})$ yields

$$\langle \tilde{v}(\ell_L, \ell_R) \rangle \simeq \tilde{v}(m\mu_{n-1}, m\mu_{n-1}) \simeq \frac{m\mu_{n-1}}{4} = 2^{d-3}\mu_{n-1}. \quad (\text{SM.8})$$

For the propagated term, linearize $\tilde{\mu}(a, b)$ at symmetry:

$$\frac{\partial \tilde{\mu}(a, b)}{\partial a} = \frac{b(b-1)}{(a+b-1)^2}, \quad \frac{\partial \tilde{\mu}(a, b)}{\partial b} = \frac{a(a-1)}{(a+b-1)^2}, \quad (\text{SM.9})$$

so at $a = b = m\mu_{n-1}$ one has $\partial \tilde{\mu} / \partial a = \partial \tilde{\mu} / \partial b = 1/4 + O(\mu_{n-1}^{-1})$. Using independence of ℓ_L, ℓ_R ,

$$\begin{aligned} \text{Var}(\tilde{\mu}(\ell_L, \ell_R)) &\simeq \left(\frac{1}{4}\right)^2 \{\text{Var}(\ell_L) + \text{Var}(\ell_R)\} \\ &= \frac{1}{16}(mv_{n-1} + mv_{n-1}) \\ &= \frac{m}{8}v_{n-1} = 2^{d-4}v_{n-1}. \end{aligned} \quad (\text{SM.10})$$

Combining (SM.8) and (SM.10) yields (8). Dividing by (SM.6) yields (9), hence $v_n/\mu_n \rightarrow 2/3$.

SM.2.5 The marginal case $d = 2$

Here $m = 2$ and the leading term in (SM.6) only gives $\mu_n \simeq \mu_{n-1}$, so we keep the next-order corrections. First,

$$\tilde{\mu}(2\mu, 2\mu) = \frac{4\mu^2}{4\mu - 1} = \mu + \frac{1}{4} + O(\mu^{-1}). \quad (\text{SM.11})$$

Second, a Taylor expansion of $\tilde{\mu}(a, b) = ab/(a+b-1)$ around $(2\mu, 2\mu)$ shows that averaging over the fluctuations of ℓ_L, ℓ_R produces a correction of order v/μ , and one finds

$$\mu_n - \mu_{n-1} \simeq \frac{1}{4} - \frac{v_{n-1}}{4\mu_{n-1}}. \quad (\text{SM.12})$$

Meanwhile, the variance recursion remains

$$v_n \simeq \frac{\mu_{n-1}}{2} + \frac{v_{n-1}}{4}, \quad (\text{SM.13})$$

so $v_n/\mu_n \rightarrow 2/3$ as before. Substituting $v_{n-1}/\mu_{n-1} \simeq 2/3$ into (SM.12) yields $\mu_n - \mu_{n-1} \simeq 1/12$, hence $\mu_n \simeq n/12 = (\log L_n)/(12 \log 2)$ and $v_n \simeq (2/3)\mu_n \simeq n/18$.

SM.3 Extension of the proof of Theorem 3 to general $d \geq 3$

This section supplies the details omitted in End Matter and derives the d -dependent constant C_d in Theorem 3. We keep the notation of End Matter. Set $m = 2^{d-1}$ as above. Note that $m = 4$ in $d = 3$. Recall the definitions of η_n and u_n in (20) and (23), and the identity (24).

SM.3.1 A concavity bound on u_n

From (23) and (17), since $(\hat{\ell}_L + 1)^{-1}$ depends only on the $m = 2^{d-1}$ variables in the left half, we may write

$$u_n = \sum_{\ell_1, \dots, \ell_m} \left(1 + \sum_{j=1}^m \ell_j\right)^{-1} \prod_{j=1}^m P_n(\ell_j), \quad (\text{SM.1})$$

where the sum is over nonnegative even ℓ_1, \dots, ℓ_m . Make the change of variables $y = (\ell + 1)^{-1} \in (0, 1]$ and define $Q_n(y) := P_n(y^{-1} - 1)$. Then $\eta_n = \sum_y y Q_n(y)$ and the above becomes

$$u_n = \sum_{y_1, \dots, y_m} \left(\sum_{j=1}^m y_j^{-1} - (m-1)\right)^{-1} \prod_{j=1}^m Q_n(y_j). \quad (\text{SM.2})$$

Fix $y_2, \dots, y_m \in (0, 1]$ and set $c := \sum_{j=2}^m y_j^{-1} - (m-1) \geq 0$. Then

$$(y_1^{-1} + c)^{-1} = \frac{y_1}{1 + cy_1} \quad (\text{SM.3})$$

is concave in $y_1 \in (0, 1]$, since its second derivative equals $-2c(1 + cy_1)^{-3} \leq 0$. Applying Jensen's inequality to the y_1 -average in (SM.2) yields

$$u_n \leq \sum_{y_2, \dots, y_m} \left(\eta_n^{-1} + \sum_{j=2}^m y_j^{-1} - (m-1) \right)^{-1} \prod_{j=2}^m Q_n(y_j). \quad (\text{SM.4})$$

Repeating the same argument for y_2, \dots, y_m gives

$$u_n \leq (m\eta_n^{-1} - (m-1))^{-1} = \frac{\eta_n}{m - (m-1)\eta_n} = \frac{\eta_n}{2^{d-1} - (2^{d-1} - 1)\eta_n}. \quad (\text{SM.5})$$

SM.3.2 A quadratic recursion for η_n

Substituting (SM.5) (with $n \mapsto n-1$) into (24) and using that $x \mapsto 2x - x^2$ is increasing on $[0, 1]$, we obtain

$$\eta_n \leq \frac{2m\eta_{n-1} - (2m-1)\eta_{n-1}^2}{(m - (m-1)\eta_{n-1})^2}. \quad (\text{SM.6})$$

A direct computation shows that for any $\eta \in [0, 1]$,

$$\begin{aligned} & \frac{2m\eta - (2m-1)\eta^2}{(m - (m-1)\eta)^2} - \left(\frac{2}{m}\eta + \left(\frac{m-1}{m} \right)^2 \eta^2 \right) \\ &= -\frac{\eta^2(\eta(m-1)^2 - m(m-2))^2}{m^2(m - (m-1)\eta)^2} \leq 0. \end{aligned} \quad (\text{SM.7})$$

Combining (SM.6) and (SM.7) yields the quadratic recursion

$$\eta_n \leq \frac{2}{m}\eta_{n-1} + \left(\frac{m-1}{m} \right)^2 \eta_{n-1}^2 = 2^{2-d}\eta_{n-1} + (1 - 2^{1-d})^2\eta_{n-1}^2. \quad (\text{SM.8})$$

SM.3.3 Iteration and the constant C_d

Let $\alpha := 2/m = 2^{2-d}$ and set

$$x_n := \alpha^{-n}\eta_n = \left(\frac{m}{2} \right)^n \eta_n = 2^{(d-2)n}\eta_n. \quad (\text{SM.9})$$

Then (SM.8) implies

$$x_n \leq x_{n-1} + \beta \alpha^{n-2} x_{n-1}^2, \quad \beta := \left(\frac{m-1}{m} \right)^2, \quad (\text{SM.10})$$

and hence

$$\frac{1}{x_n} \geq \frac{1}{x_{n-1}} - \beta \alpha^{n-2}, \quad (\text{SM.11})$$

since $(x + ax^2)^{-1} \geq x^{-1} - a$ for $x > 0$ and $a \geq 0$. Summing and using $x_0 = \eta_0 = (A_0 + 1)^{-1}$ yields

$$\frac{1}{x_n} \geq (A_0 + 1) - \beta \sum_{j=1}^n \alpha^{j-2} \geq (A_0 + 1) - \frac{\beta}{\alpha(1-\alpha)} = (A_0 + 1) - \frac{(m-1)^2}{2(m-2)}. \quad (\text{SM.12})$$

Therefore

$$\eta_n^{-1} = \alpha^{-n}x_n^{-1} \geq \left(A_0 + 1 - \frac{(m-1)^2}{2(m-2)} \right) \left(\frac{m}{2} \right)^n = \left(A_0 + 1 - \frac{(2^{d-1} - 1)^2}{2(2^{d-1} - 2)} \right) 2^{(d-2)n}. \quad (\text{SM.13})$$

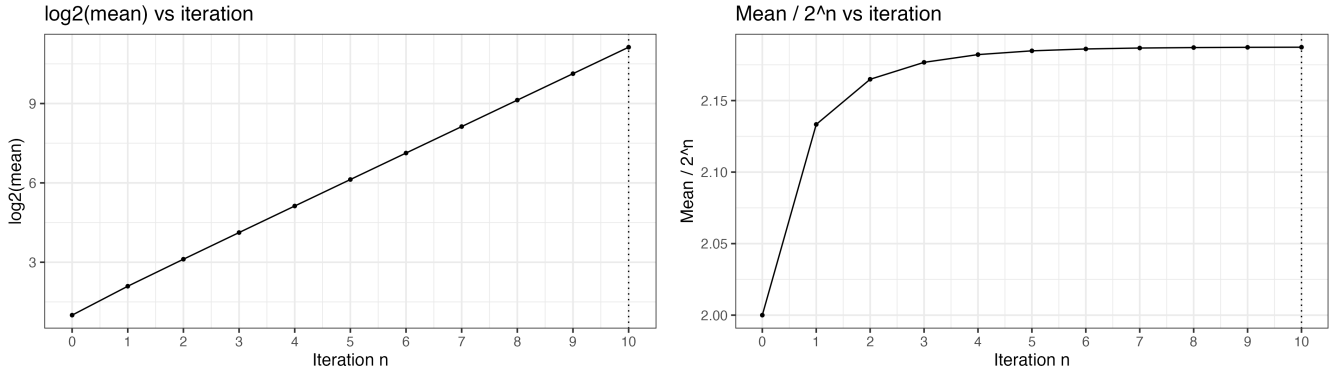


FIG. SM.2. (3D Hierarchical model) Mean conductance μ_n in $d = 3$ with initial crossing $A_0 = 2$. Left: $\log_2 \mu_n$ versus iteration $n = \log_2 L_n$. The linear growth is consistent with the normal-transport scaling $\mu_n \propto L_n = 2^n$. Right: As n increases, the ratio $\mu_n/2^n$ converges to a constant (the conductivity).

Since $A_n/L_n = A_0 2^{(d-2)n}$ and $\mu_n \geq \eta_n^{-1} - 1$, we conclude

$$\mu_n \geq \left[1 - \frac{1}{A_0} \left(\frac{(2^{d-1} - 1)^2}{2(2^{d-1} - 2)} - 1 \right) \right] \frac{A_n}{L_n} - 1, \quad (\text{SM.14})$$

which is exactly the bound stated in Theorem 3 (with the constant C_d given there).

SM.4 Numerical simulations

The present section provides additional information on our numerical work. We focus on the hierarchical Lorentz mirror model, where the recursion (2) can be iterated essentially exactly (i.e., without Monte Carlo sampling), and we briefly discuss the original (non-hierarchical) Lorentz mirror model in the final subsection.

SM.4.1 The set-up and codes for the hierarchical recursion

Recall that $P_n(\ell)$ (with $\ell \in 2\mathbb{Z}_{\geq 0}$) denotes the probability that the generation- n block has exactly ℓ crossings. It is determined by the recursion (2), where the kernel $K(\ell | \ell_L, \ell_R)$ is given by (3).

We provide two codes for iterating the recursion:

- **scramblers.cpp** (2D): iterates (2) with $d = 2$, i.e. $m := 2^{d-1} = 2$ subblocks in parallel per half.
- **scramblers3d.cpp** (3D): iterates (2) with $d = 3$, i.e. $m := 2^{d-1} = 4$ subblocks in parallel per half.

To be more precise, we first compute the m -fold convolution

$$P_{n-1}^{*m}(\ell') := \sum_{\substack{\ell_1, \dots, \ell_m \\ (\sum_{j=1}^m \ell_j = \ell')}} \prod_{j=1}^m P_{n-1}(\ell_j), \quad (\text{SM.1})$$

and then evaluate the next-generation distribution via

$$P_n(\ell) = \sum_{\ell_L, \ell_R} K(\ell | \ell_L, \ell_R) P_{n-1}^{*m}(\ell_L) P_{n-1}^{*m}(\ell_R). \quad (\text{SM.2})$$

In both codes, the full law on even integers is stored as an array, $\text{prob}[k] = \text{Prob}(\hat{\ell}_n = 2k)$, and the recursion (2) is evaluated directly. Very small probabilities (below a pruning threshold $\simeq 10^{-18}$) are discarded to keep the support finite. In our implementation, the total discarded mass is negligible at the scale of the reported observables; after pruning we renormalize the distribution to have unit total mass.

The codes output the mean $\mu_n = \langle \hat{\ell} \rangle_n$, the variance $v_n = \langle (\hat{\ell} - \mu_n)^2 \rangle_n$, and their ratio v_n/μ_n . No Monte Carlo sampling is used: apart from the pruning step just described, the computation is exact.

As in the main text, we set the initial distribution as $P_0(\ell) = \delta_{\ell, A_0}$, where A_0 is a positive even integer. In the $d = 3$ plots below we use $A_0 = 2$, while in the $d = 2$ plots we use $A_0 = 90$ (see the discussion below).

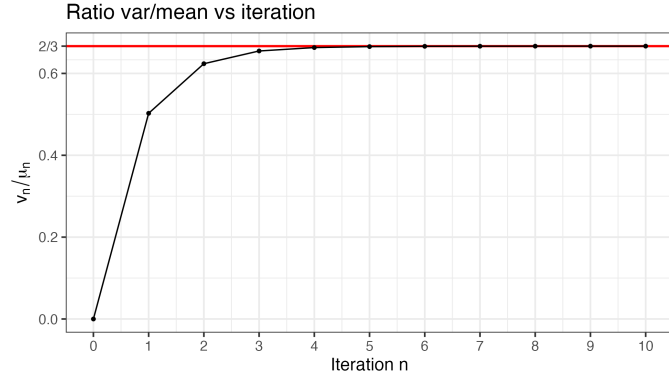


FIG. SM.3. (3D Hierarchical model) Ratio v_n/μ_n versus iteration $n = \log_2 L_n$ in $d = 3$ with initial crossing $A_0 = 2$. The ratio converges quickly toward $2/3$ (thick red line).

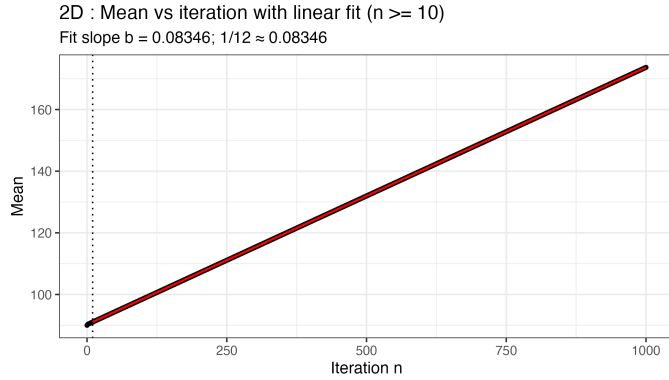


FIG. SM.4. (2D Hierarchical model) Mean conductance $\mu_n = \langle \hat{\ell} \rangle_n$ versus iteration $n = \log_2 L_n$ in $d = 2$ with initial crossing $A_0 = 90$. A linear regression fit for $n \geq 10$ yields the slope $b \simeq 0.08346$, which is indistinguishable from $1/12$.

SM.4.2 Results in $d = 3$: normal-conductance scaling and the $2/3$ law

In $d = 3$, we proved that the mean conductance μ_n grows proportionally to 2^n for any $A_0 \geq 2$. Here we choose the smallest initial crossing number and set $A_0 = 2$.

Figure SM.2 shows $\log_2 \mu_n$ and $\mu_n/2^n$ as functions of the generation n . The behavior is consistent with normal-transport scaling. Note that the conductivity $\kappa := \lim_{n \uparrow \infty} \mu_n/L_n$ (read off from the right panel) is nonuniversal and depends on the initial distribution P_0 .

From the Gaussian closure, we expect the variance-to-mean ratio v_n/μ_n to converge to the universal constant $2/3$. Figure SM.3 shows v_n/μ_n for $n \leq 10$. The ratio rapidly approaches a plateau very close to $2/3$ (already by $n \simeq 6$), providing clean numerical support for the $2/3$ mean-variance law in $d = 3$.

SM.4.3 Results in $d = 2$: logarithmic growth and the $2/3$ law

In the marginal dimension $d = 2$, the Gaussian closure predicts a slow growth of the mean conductance, $\mu_n \simeq n/12$, equivalently $\mu_n \simeq (\log L_n)/(12 \log 2)$, as in (10).

If we start from the smallest crossing number $A_0 = 2$, we observe the expected slow growth, but the distribution $P_n(\ell)$ is then essentially supported only on small values of ℓ . (For example, $P_{100}(\ell)$ is almost negligible for $\ell \geq 20$.) In this regime, measures of “distance to Gaussianity” are strongly affected by discreteness.

To reduce such discreteness effects, we choose here a larger initial crossing number, $A_0 = 90$. Then, after a single application of the recursion (2), we obtain $P_1(\ell) = K(\ell | 180, 180)$, which is already close to a Gaussian by the asymptotics of the kernel.

Figure SM.4 shows μ_n versus n , together with a linear regression for $n \geq 10$. The best-fit slope is

$$\mu_n \simeq a + b n \quad (\text{as } n \uparrow \infty), \quad b \simeq 0.08346, \quad (\text{SM.3})$$

which essentially coincides with the Gaussian-closure prediction $b = 1/12 = 0.08333 \dots$.

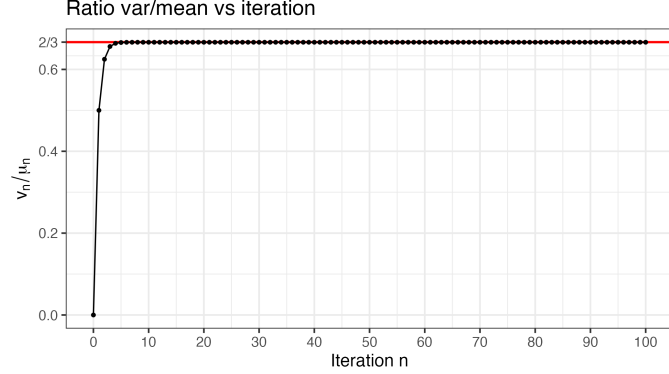


FIG. SM.5. (2D Hierarchical model) Ratio v_n/μ_n versus iteration $n = \log_2 L_n$ in $d = 2$ with initial crossing $A_0 = 90$. The thick red line marks the target value $2/3$.

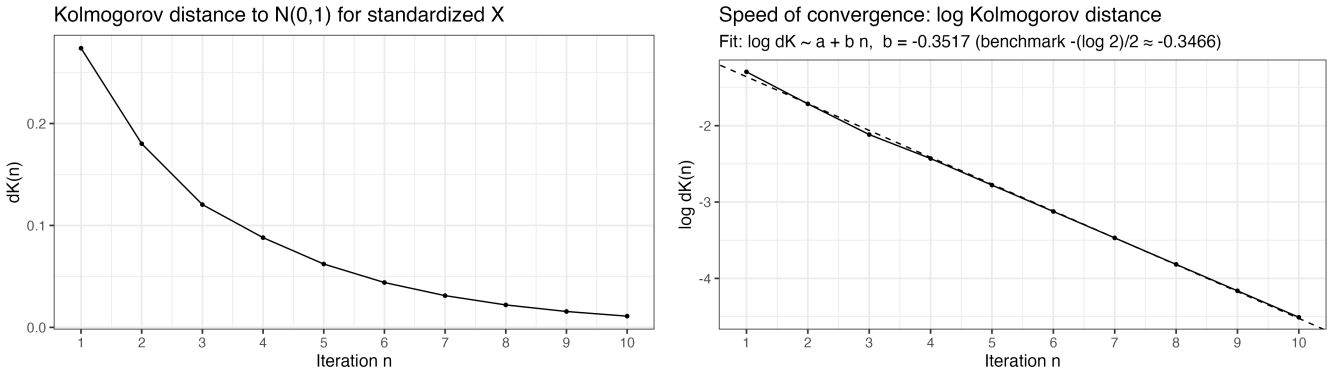


FIG. SM.6. (3D Hierarchical model) Left: Kolmogorov distance $d_K(n)$ defined in (SM.5) between the standardized iterate Z_n and $\mathcal{N}(0, 1)$. The distance decreases rapidly with n . Right: $\log d_K(n)$ versus n with a linear fit. The fitted slope (dashed line) $b \simeq -0.3517$ is close to $-(\log 2)/2 \simeq -0.3466$, suggesting $d_K(n) \simeq 2^{-n/2}$ as $n \uparrow \infty$.

The variance-to-mean ratio v_n/μ_n is also well behaved. As shown in Fig. SM.5, v_n/μ_n stabilizes near the universal value $2/3$ after only a short transient.

SM.4.4 Convergence to Gaussianity in $d = 3$

As mentioned in the main text, for the hierarchical model with $d = 3$ the distribution P_n rapidly approaches a Gaussian shape as n grows. To quantify this, we use the Kolmogorov distance between the standardized crossing number and the standard normal distribution.

Let $\hat{\ell}_n$ denote the number of crossings in the generation- n block and define the standardized variable

$$Z_n := \frac{\hat{\ell}_n - \mu_n}{\sqrt{v_n}}. \quad (\text{SM.4})$$

Let $F_n(z) = \text{Prob}[Z_n \leq z]$ be the cumulative distribution function (CDF) of Z_n , and let $\Phi(z)$ be the CDF of the standard normal $\mathcal{N}(0, 1)$. We define the Kolmogorov distance by

$$d_K(n) := \sup_{z \in \mathbb{R}} |F_n(z) - \Phi(z)|. \quad (\text{SM.5})$$

As shown in the left panel of Fig. SM.6, $d_K(n)$ decreases quickly over the first few iterations and reaches the percent level by $n \simeq 10$. A linear fit of $\log d_K(n)$ versus n (right panel) yields

$$\log d_K(n) \simeq a + b n \quad (\text{as } n \uparrow \infty), \quad b \simeq -0.3517. \quad (\text{SM.6})$$

This demonstrates exponential convergence of the standardized law to $\mathcal{N}(0, 1)$ in the $d = 3$ hierarchical model.

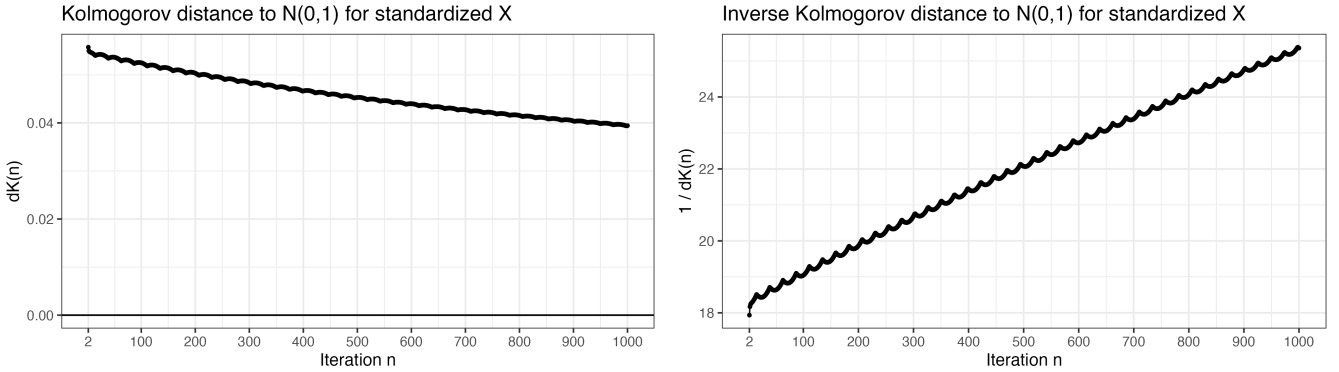


FIG. SM.7. (2D Hierarchical model) Left: Kolmogorov distance $d_K(n)$ defined in (SM.5) between the standardized iterate Z_n and $\mathcal{N}(0,1)$. The distance decreases slowly with n . Right: $1/d_K(n)$ versus n exhibits an approximately linear growth, indicating $d_K(n) \propto n^{-1}$ at large n . Mild oscillations visible in the data are due to the lattice nature of ℓ and are not essential.

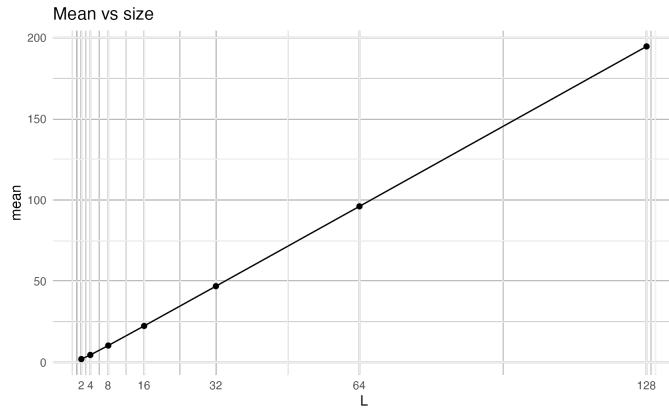


FIG. SM.8. (3D Original model) Mean conductance $\bar{\mu}(L)$ versus system size L in the original Lorentz mirror model in $d = 3$. Our preliminary laptop-scale simulations are consistent with the linear growth predicted by normal transport (1). For comparison, Fig. 6 of [17] reports large-scale simulations of $\bar{\mu}(L)/L$ for L from 5 to 420.

Noting that the estimated slope is close to $-(\log 2)/2$, we are led to conjecture

$$d_K(n) \simeq C 2^{-n/2} \propto \frac{1}{\sqrt{\mu_n}}, \quad (\text{SM.7})$$

as $n \uparrow \infty$.

SM.4.5 Slow convergence to Gaussianity in $d = 2$

Let us turn to the case $d = 2$, where we set $A_0 = 90$. Recall that $P_1(\ell) = K(\ell | 180, 180)$ is already close to a Gaussian.

As can be seen in the left panel of Fig. SM.7, the Kolmogorov distance $d_K(n)$ decays very slowly with n . The plot of $1/d_K(n)$ in the right panel suggests that $d_K(n)$ decays proportionally to $1/n$ for large n .

We shall study the approach of $P_n(\ell)$ to a Gaussian perturbatively in [SM1].

SM.4.6 The original Lorentz mirror model in $d = 3$

As explained in the main text, we performed preliminary simulations of the original Lorentz mirror model on the $L \times L \times L$ cubic lattice for $L = 2^n$ with $n = 1, \dots, 7$. Our codes (which generate quenched random environments with local pairings and count the resulting number of crossings) are:

- `cross_stats.cpp` and `cross_stats_rect.cpp`.

For each L and each of the two local pairing rules described in the main text, we generated $M = 6.4 \times 10^5$ independent environments. For a given environment, we faithfully computed the conductance \mathcal{C} (the number of left-right crossings)

by tracing deterministically the trajectories of particles injected from all L^2 external edges on the left boundary and recording their exit edges. From these data we estimated the mean $\bar{\mu}(L) = \langle \mathcal{C} \rangle$ and the variance $\bar{v}(L) = \langle (\mathcal{C} - \bar{\mu}(L))^2 \rangle$, together with 95% confidence intervals.

Uncertainties are obtained by a block (batching) analysis: the M environments are split into K blocks, and the dispersion of block-level estimators provides the standard error and corresponding normal confidence intervals. Since the generation of an environment requires specifying L^3 local pairings and the subsequent trajectory tracing is of comparable cost, the runtime increases rapidly with L ; for $L = 128$ the total computation time is about 2.5×10^4 s on a laptop.

The key outcome of the simulations is the approach of $\bar{v}(L)/\bar{\mu}(L)$ to the universal value $2/3$, shown in Fig. 3 of the main text. Figure SM.8 provides complementary evidence that our preliminary simulations are consistent with the normal-transport scaling (1) in $d = 3$. We stress that decisive numerical evidence for (1) is provided by the large-scale simulations in [17].

Reference

[SM1] R. Lefevere and H. Tasaki, “Hierarchical Lorentz mirror model: a perturbative approach”, in preparation.